arXiv:cond-mat/0110319v1 [cond-mat.mtrl-sci] 16 Oct 2001

A Model for Isotropic Crystal Growth from Vapor on a Patterned Substrate

M. Khenner[1] R.J. Braun[1] and M.G. Mauk[2]

[1] Department of Math. Sciences
University of Delaware, Newark, DE 19716

[2] AstroPower, Inc.
Solar Park, Newark, DE 19716

February 1, 2008

Abstract

We developed a consistent mathematical model for isotropic crystal growth on a substrate covered by the mask material with a periodic series of parallel long trenches where the substrate is exposed to the vapor phase. Surface diffusion and the flux of particles from vapor are assumed to be the main mechanisms of growth. A geometrical approach to the motion of crystal surface in two dimensions is adopted and nonlinear evolution equations are solved by a finite-difference method. The model allows the direct computation of the crystal surface shape, as well as the study of the effects due to mask regions of effectively nonzero thickness. As in experiments, lateral overgrowth of crystal onto the mask and enhanced growth in the region near the contact of the crystal and the mask is found, as well as the comparable crystal shapes. The growth rates in vertical and lateral directions are investigated.

Keywords: selective epitaxy, vapor phase epitaxy, computer simulation.

1 Introduction

Selective area growth (SAG) of compound semiconductor thin films by (metalorganic) vapor phase epitaxy on patterned, masked substrates is a useful technique for fabricating semiconductor devices [1]-[3]. The masked substrates may also be used as a diagnostic tool; the crystals grown in artificial geometries may indicate what would be successful or unsuccessful conditions for producing a desired product. The masked substrates may also be used simply for fundamental understanding of the crystal growth process [3]-[11].

Generally, the method consists of the deposition of an epitaxial layer on defined areas of the substrate, which are exposed to the vapor phase via windows lithographically etched

through a masking layer. For semiconductor device processing the mask is usually a dielectric material such as SiO_2 or Si_3N_4. In some cases, crystal growth on the mask is not desirable but, in reality, growth is observed there more often than not [3, 5, 9], [12]-[14]. The growth on the mask may occur via lateral overgrowth from the window in the mask or via nucleation on the mask; the narrower the mask the less likely is nucleation. Following [6], we will denote the lateral overgrowth phenomena as "epitaxial lateral overgrowth" (ELOG) in case of growth in narrow windows (< 10 μm in width). We refer to the selective growth on larger areas (hundreds of microns) as SAG.

In SAG and ELOG the overall growth rate and uniformity of the epitaxial deposit have been reported to be strongly dependent upon the geometry of masked regions [3] as well as the total pressure [10, 11, 15, 16]. In addition, the deposits are characterized by an enhanced growth at the perimeter of the windows adjacent to the mask (excellent photographs of the enhanced growth and the ELOG regions of GaInAs(P) and InP can be found in [3], for example). This suggests that material is supplied to the unmasked areas by surface diffusion along the mask as well as through direct diffusion from the vapor phase. It is generally concluded that diffusion lengths on the mask and on the surface of the epitaxial material such as GaAs, Si or GaN are very short (of the order of 1 μm). Under these conditions, the dominant lateral mass transport mechanism from the mask regions, for distances greater than a few (say 10) microns, is usually attributed to vapor-phase diffusion [5, 6, 7], [9]-[11]. However, surface diffusion usually dominates [6, 7, 11, 17, 18] for the growth in narrow windows bounded by narrow mask regions (< 10 microns) and it is this case (ELOG) that we are interested in studying.

In our opinion, there exist two types of mathematical models for the selective-area growth. Type 1 models operate by solving Laplace's [3, 8, 19] or the diffusion equation [20] for the concentration of species in the vapor phase, subject to appropriate boundary conditions. The solution yields the concentration profiles in the vapor. Surface diffusion is ignored in these models.

Type 2 models attempt to account for surface diffusion in several ways. In [9], the steady-state diffusion equation for the concentration of species on the mask is added to the Laplace's equation in the vapor, while the diffusion on the crystal surface is ignored. In [17], the time-dependent diffusion equation for the concentration of species on the crystal surface is considered, while the diffusion on the mask is ignored. In [18], the steady-state diffusion equation describes diffusion on both the mask and crystal surfaces, again with appropriate boundary conditions.

Neither Type 1 nor Type 2 models allow the overgrowth of the crystal on the mask (except [9]), nor do they account for the topography of the mask (i.e., the mask is considered to be of zero thickness). They also do not compute the crystal surface shape. As far as we know, the anisotropic selective-area growth has not been modeled.

The goal of this paper is to give a physically and mathematically consistent description of epitaxial semiconductor crystal growth on a masked substrate in a surface diffusion-limited regime. The model is based on two partial differential equations; one for the crystal surface dynamics and one for the surface concentration of atoms on the mask. The substrate is exposed in the periodic series of parallel long trenches etched in the mask. Diffusion in the vapor phase is ignored since we consider ELOG in this study. Other simplifying assumptions

are:

- The perturbations caused by selective-area epitaxy are independent of the orientation of the trenches with respect to the crystallographic axes of the substrate. In other words, in this study we ignore the anisotropy of the crystal growth (the results for the anisotropic growth will be reported elsewhere [21]);

- The diffusion coefficients are constants. It means that we have also assumed that the temperature is constant over the calculation window. The assumption of the constant temperature seems reasonable since we consider the case of the growth on narrow regions of the substrate (as explained above);

- The (possible) interaction between densely arrayed growth regions is ignored. The numerical methodology we make use of in this study is not suitable for the latter problem. Other numerical methods (such as the level set method [22]) should be employed to study the crystal surfaces originating from different growth regions beyond the point of their merging.

The model is designed to allow the direct computation of the crystal surface shape. In addition, it allows to study effects due to mask regions of effectively nonzero thickness.

The equations and added physical boundary conditions and initial conditions are nondimensionalized using physical constants estimated for experiments on ELOG and SAG of GaAs-type materials [23]-[25]. A finite difference method is used to find approximate solutions to the nondimensionalized, fully nonlinear parametric evolution equations which govern the crystal surface dynamics. The numerical solutions exhibit the crystal overgrowth onto the mask and enhanced growth in the region adjacent to the contact point (a contact line in three dimensions) where the mask and the crystal surfaces meet.

The outline of the paper is as follows. In Section 2 we formulate the mathematical model, list physical constants, provide details of nondimensionalization and find an approximate solution to the problem for diffusion of the concentration on the mask. In Section 3 we describe the numerical method we use to solve the nonlinear initial/boundary value problem for the crystal/vapor interface. In Section 4 we present the numerical results for the ELOG in the assumption of nonzero thickness of the mask. By setting mask thickness to zero we obtain more representative results in Section 5. Finally, in Section 6 we provide the qualitative comparison of the results obtained to the existing results we found in the literature and give conclusions and future directions for research.

2 Mathematical model

In this section, we describe the mathematical model which is an initial/boundary value problem consisting of two partial differential equations, one describing the surface concentration of the atoms on the mask and the other involving the motion of the crystal/vapor interface originating from the exposed substrate. We also introduce physical constants and use them to nondimensionalize the problem. This model development was partly given in [4].

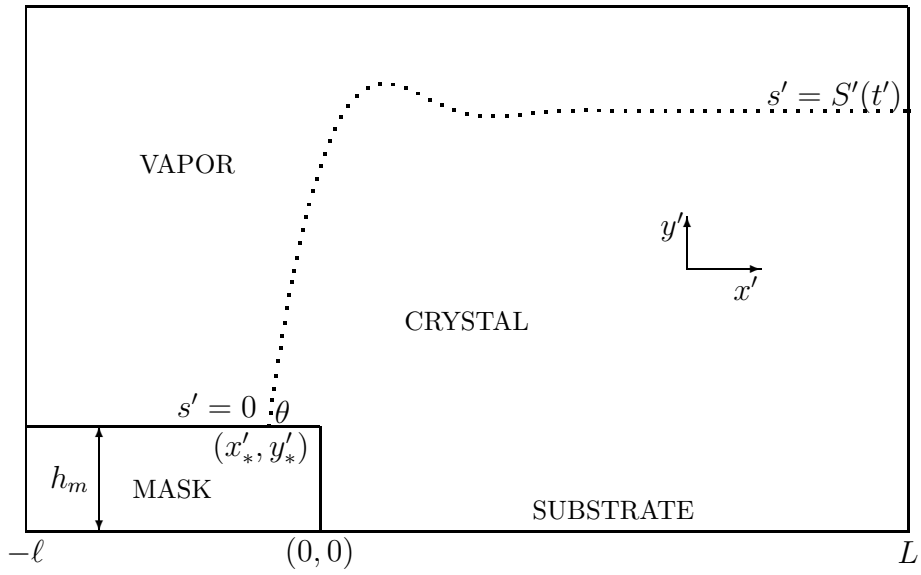

Figure 1: A sketch of the mathematical situation. The free surface of the growing crystal (curve in two dimensions) is defined parametrically as $y' = y'(s',t')$, $x' = x'(s',t')$, $0 \le s' \le S'(t')$, where s' is the arc length along the curve and S' is the total arc length of the curve. The surface is sketched such that a crystal overgrowth onto the mask and the region of the enhanced growth ("bump") near the contact point are shown.

2.1 Surface diffusion over the mask

Our study is on the flat surface covered by the mask material with a periodic series of parallel long trenches where the substrate is exposed. We examine the growth behavior on a partial cross-section which is a line segment extending from the center line of one of the masked "plateaus" to the center of the next trench; a sketch of the mathematical situation is given in Figure 1. We assume the surface behavior is constant in the perpendicular direction to legitimize this two-dimensional study.

The interval $-\ell \le x' \le 0$ corresponds to the zone where the thin mask is located. Here we study the surface diffusion of the concentration $n_m = n_m(x',t')$ of atoms on the horizontal part of the mask not yet occupied by the growing crystal:

$$\frac{\partial n_m}{\partial t'} = D_s^{(m)} \frac{\partial^2 n_m}{\partial (x')^2} + J_g - \frac{n_m}{\tau_m}, \quad -\ell \le x' \le x'_*(t') \tag{2.1}$$

where, J_g represents uniform flux of atoms from a vapor and impinging on the mask. The term n_m/τ_m provides the concentration of atoms leaving the surface to go into the vapor. The constant τ_m is the mean residence time on the step. Finally, $D_s^{(m)}$ is the surface diffusivity of the atomic concentration on the mask. Note that (2.1) has been given in [23, 24], for example.

Appended to (2.1) is a symmetry boundary condition,

$$\frac{\partial n_m}{\partial x'}(-\ell, t') = 0. \tag{2.2}$$

We assume that the atoms close to the crystal will be absorbed quickly; thus we take the boundary condition at the contact point to be a perfect sink:

$$n_m(x'_*(t'), t') = 0. \tag{2.3}$$

An initial condition is also needed to define this part of the problem completely, say

$$n_m(x', 0) = 0, \quad -\ell \le x' \le 0. \tag{2.4}$$

To summarize, there exist two options for every atom arriving to the horizontal part of the *macroscopic* step which represents the mask at $-\ell \le x' \le 0$: it can either desorb back into the vapor phase or be transported by surface diffusion from left to right. The drifting atoms are incorporated in the crystal at the contact point (x'_*, y'_*) as they meet the crystal on the way. At the initial stage of the growth the atoms need to diffuse over the mask corner prior to being incorporated in the crystal. We don't study surface diffusion along the vertical part of the step and assume that atoms diffused over the corner are incorporated in the growing crystal instantly. This approximation is good if the mask thickness is much less than the mask region width, that is if $h_m \ll \ell$ (in ELOG the ratio h_m/ℓ is usually < 0.1 [3, 5, 7], [11]-[15], [17]. In SAG this ratio is so small that the mask can be considered to be of vanishing thickness). Both parts of the mask are assumed to be physically equivalent. As a particular consequence, the constant equilibrium angle $\theta(\gamma, \gamma_m)$ which the crystal surface forms with the mask at the contact point (as a result of the assumed thermodynamic equilibria in the vicinity of the junction [26]; γ and γ_m are the surface energies of the crystal and of the mask respectively) should be the same and independent of the contact point position on the step, ref. Figure 1.

2.2 Model for the crystal surface

We now turn to the formulation of the equations and the associated boundary and initial conditions for the motion of the interface between the crystal that is built-up from the substrate on the interval $0 \le x' \le L$ and the vapor. The interface is allowed to move above the mask on the interval $-\ell \le x' < 0$. This development of the model closely parallels that of Mullins [27] in his now classic study of grain boundary grooving.

The interface moves via two mechanisms. The first is from a flux of atoms to the interface from the vapor; this flux is normal to the interface. This contribution to the normal velocity of the interface is proportional to the jump in the chemical potential across the interface, viz.,

$$MA(\mu_V^T - \mu_c). \tag{2.5}$$

Here M is the mobility of the interface and $A = \partial n_s/\partial\mu$ is the change of surface concentration n_s with chemical potential μ; μ_c is chemical potential of the crystal surface and is given by

$$\mu_c = \mu_\infty + \Omega\gamma\kappa, \tag{2.6}$$

where γ is the surface energy of the crystal, Ω is the atomic volume, κ is the curvature of the crystal surface and μ_∞ is the reference value of the chemical potential for the crystal with a flat surface. μ_V^T is the chemical potential of the vapor and it may be written as $\mu_V^T = \mu_V + \mu_\infty$. Comparison with [27] reveals that A plays a role identical to n_s/kT, where n_s is the surface concentration, k is Boltzmann's constant, and T is the absolute temperature.

The second contribution is from the surface diffusion of atoms along the interface; the current of atoms J_s is proportional to the gradient of the chemical potential along the surface. For the curve in the plane, the surface gradient is the derivative with respect to arc length, hence

$$J_s = -AD_s^{(c)} \frac{\partial \mu_c}{\partial s'}. \tag{2.7}$$

The contribution to the rate of increase in the atoms per unit area (proportional to the normal velocity) is proportional to the surface divergence of this flux; for the curve, we have $(-\partial J_s/\partial s')$.

The net rate of increase in the number of atoms per unit area (or the time rate of change of the concentration) may be written as V_n'/Ω, where the Ω is the atomic volume and V_n' is the normal velocity. Combining the normal and surface diffusion contributions results in

$$V_n' = A\Omega \left\{ \frac{\partial}{\partial s'} \left[D_s^{(c)} \frac{\partial}{\partial s'} (\Omega \gamma \kappa) \right] + M(\mu_V - \Omega \gamma \kappa) \right\}. \tag{2.8}$$

The parametric evolution equations for the crystal surface are given in the Section 2.2.1. Next, we describe physical boundary and initial conditions which will be used for the computation.

First, we assume the following obvious conditions hold for the contact point location x_*', y_*' (see Figure 1):

$$\begin{aligned} x_*' &= 0, \quad \text{if} \quad 0 \le y_*' < h_m, \\ y_*' &= h_m, \quad \text{if} \quad -\ell \le x_*' < 0. \end{aligned} \tag{2.9}$$

These conditions place the contact point on the mask.

At $x' = L$ we assume the symmetry conditions,

$$\frac{\partial y'}{\partial x'}(L, t') = 0 \ \text{ and } \ \frac{\partial^3 y'}{\partial (x')^3}(L, t') = 0. \tag{2.10}$$

In (2.10), the second condition is effectively the condition of no atomic flux at $x = L$ [27].

Unless otherwise noted, the crystal surface is initially a horizontal line even with the substrate,

$$y'(x', 0) = 0, \quad 0 \le x' \le L. \tag{2.11}$$

After the short time the crystal rearranges to form an equilibrium angle θ with the mask at the contact point:

$$\begin{aligned} t' > 0: \quad & \frac{\partial y'}{\partial x'}|_{(x_*', y_*')} = \tan\theta, \quad \text{if} \quad -\ell \le x_*' < 0 \ \text{ and } \ y_*' = h_m, \\ & \frac{\partial y'}{\partial x'}|_{(x_*', y_*')} = \tan(\theta - 90^\circ), \quad \text{if} \quad x_*' = 0 \ \text{ and } \ 0 \le y_*' < h_m. \end{aligned} \tag{2.12}$$

We also match the fluxes from the atoms on the mask surface moving from left-to-right with the flux onto the growing crystal by requiring that

$$D_s^{(m)} \frac{\partial n_m}{\partial x'}(x'_*, t') = A D_s^{(c)} \Omega \gamma \frac{\partial \kappa}{\partial s'}(x'_*, t'). \tag{2.13}$$

2.2.1 Evolution equations for the crystal surface

We take a geometrical approach to the problem of the motion of an open curve (crystal surface) $\gamma(t')$ along it's normal vector field with a speed function of curvature and some of it's derivatives.

Let $\mathbf{x}'(r, t')$ be the position vector which, at time t', parametrizes $\gamma(t')$ by r, $0 \leq r \leq R(t')$ (r is not necessarily the arc length). With $\kappa(r, t')$ as the curvature at $\mathbf{x}'(r, t')$, the equations of motion are

$$\begin{gathered} \mathbf{n}(r, t') \cdot \frac{\partial \mathbf{x}'(r, t')}{\partial t'} = V'_n(\kappa(r, t'), \kappa_r, ...), \\ \mathbf{x}'(r, 0) = \gamma(0) \quad \text{prescribed}, \end{gathered} \tag{2.14}$$

where $\mathbf{n}(r, t') = -\mathbf{i}\ \partial y'/\partial r + \mathbf{j}\ \partial x'/\partial r$ is the unit normal vector at $\mathbf{x}'(r, t')$ and $\mathbf{i}$ and $\mathbf{j}$ are the unit vectors along x and $y-$axis respectively.

Written in terms of the coordinates $\mathbf{x}'(r, t') = (x'(r, t'), y'(r, t'))$, an equivalent formulation is [28]

$$\begin{aligned} \frac{\partial x'}{\partial t'} &= V'_n \frac{1}{g'} \frac{\partial y'}{\partial r}, \\ \frac{\partial y'}{\partial t'} &= -V'_n \frac{1}{g'} \frac{\partial x'}{\partial r}, \end{aligned} \tag{2.15}$$

where

$$g' = \sqrt{\left(\frac{\partial x'}{\partial r}\right)^2 + \left(\frac{\partial y'}{\partial r}\right)^2} \tag{2.16}$$

is metric function (the metric function measures the "stretch" of the parametrization). The relation

$$ds' = g'(r, t)\ dr \tag{2.17}$$

can be used to cast the normal velocity (2.8) in terms of r. The expression for the curvature in terms of x', y' is

$$\kappa = \frac{1}{(g')^3} \left(\frac{\partial^2 y'}{\partial r^2} \frac{\partial x'}{\partial r} - \frac{\partial^2 x'}{\partial r^2} \frac{\partial y'}{\partial r} \right). \tag{2.18}$$

2.3 Physical parameters

The physical constants listed in Table 1 are representative for ELOG of GaAs-type materials at temperatures near 650 K.

Since the parameter space is large, the parameters in Table 1 were fixed in the course of our study of ELOG. We only investigated the influence of the four geometrical parameters, L, ℓ, h_m and θ. These parameters (except θ) can be controlled in the experiment given the epitaxial material and growth conditions; changing materials changes θ. We varied L, ℓ, h_m and θ within the intervals listed in Table 2.

Table 1: Physical constants.

Constant	Description	Value/Units
J_g	Atomic flux from vapor	10^{15} Atoms/(cm^2·sec)
τ_m	Mean residence time of atoms on mask	1 sec
$D_s^{(m)}$	Diffusivity on mask	5×10^{-8} cm^2/sec
$D_s^{(c)}$	Diffusivity on crystal surface	2×10^{-8} cm^2/sec
Ω	Atomic Volume	2×10^{-23} cm^3/Atom
γ	Surface energy	10^3 ergs/cm^2
A	Change in concentration/Change in chemical potential	2×10^{28} Atoms^2/(erg·cm^2)
μ_V	Chemical potential in the vapor	3×10^{-13} erg $\cdot$ atom
M	Mobility	10 sec^{-1}

Table 2: Geometrical parameters.

Parameter	Description	Value/Units
L	Width of substrate region	$10^{-4} - 10^{-3}$ cm $(1 - 10\ \mu$m$)$
ℓ	Width of mask region	$10^{-4} - 10^{-3}$ cm $(1 - 10\ \mu$m$)$
h_m	Height of mask above substrate	$0 - 1.25 \times 10^{-4}$ cm $(0 - 1.25\ \mu$m$)$
θ	Contact angle	$0^\circ - 180^\circ$

Table 3: Nondimensional parameters.

Constant	Expression	Approximate Value (for $L = \ell = 5$ μm)
ϵ	$D_s^{(c)}/D_s^{(m)}$	4×10^{-1}
D	$(\Omega^2 A\gamma)/(L^2)$	3×10^{-8}
δ	$(M\Omega^2\gamma A)/D_s^{(m)}$	1.6×10^{-6}
α	$L^2/(\tau_m D_s^{(m)})$	5
J	$(\Omega A\mu_V ML)/D_s^{(m)}$	1.2×10^{-2}
$\bar{h}_m$	h_m/L	10^{-1}
β	$(A\Omega\gamma)/(\tau_m J_g L)$	8×10^{-4}
d	ℓ/L	1
f_m	$\sqrt{\alpha}\tanh(\sqrt{\alpha}d)$	2.18

2.4 Nondimensionalization and diffusion problem over the mask

To complete this section we now describe the nondimensionalization used and solve the problem for the concentration on the mask. Table 3 has all the nondimensional parameters.

As above, we first handle the diffusion problem over the mask. Letting

$$x' = Lx, \quad t' = \frac{L^2}{D_s^{(m)}}t, \text{ and } n_m = \tau_m J_g u$$

we can rewrite (2.1)-(2.4) as

$$\frac{\partial u}{\partial t} = \frac{\partial^2 u}{\partial x^2} + \alpha(1-u), \quad -d \le x \le x_*(t) \tag{2.19}$$

with boundary conditions

$$\frac{\partial u}{\partial x}(-d,t) = 0 \text{ and } u(x_*(t),t) = 0 \tag{2.20}$$

and an initial condition

$$u(x,0) = 0. \tag{2.21}$$

When the contact point position is fixed at $x_*(t) = 0$, an exact solution to the problem (2.19) - (2.21) may be found [4]. In that case, a constant flux may be found from the steady state solution to (2.19) (with $x_*(t) = 0$). This constant flux is given by

$$\frac{\partial u_{steady}}{\partial x}(x) = -\sqrt{\alpha}\left(\sinh(\sqrt{\alpha}x) + \tanh(\sqrt{\alpha}d)\cosh(\sqrt{\alpha}x)\right); \tag{2.22}$$

At $x = 0$ we have

$$\frac{\partial u_{steady}}{\partial x}(0) = -\sqrt{\alpha}\tanh(\sqrt{\alpha}d). \tag{2.23}$$

The value of $f_m \equiv |\frac{\partial u_{steady}}{\partial x}(0)|$ is estimated to be 2.18 for the parameters in Table 3. When the contact point moves, the same steady flux is not available; however, we will assume a constant flux f_m from the mask at the contact point for the rest of this paper. The flux f_m will be used as a boundary condition for the evolution equations of the growing crystal. The approximation just described is validated in [21], where we numerically solve the full surface diffusion problem on the mask and demonstrate that the contact point indeed propagates steadily along the mask.

We also can estimate the effect of neglecting surface diffusion along the vertical part of the step. If we replace d with $d + \bar{h}_m$ in the expression (2.23) for the steady flux at the contact point, the resulting change in f_m will be very small since $\bar{h}_m \ll d$ for ELOG (ref. Table 3).

To nondimensionalize (2.8)-(2.13), (2.15)-(2.18) we make the following variable changes, again referring to Table 3 for the definitions of the nondimensional parameters:

$$y' = Ly,\ x' = Lx,\ s' = Ls,\ g' = Lg,\ h_m = L\bar{h}_m,\ \kappa = L^{-1}K \ \text{ and } \ t' = \frac{L^2}{D_s^{(m)}}t.$$

The evolution equations then become

$$\frac{\partial x}{\partial t} = V_n \frac{1}{g} \frac{\partial y}{\partial r}, \tag{2.24}$$

$$\frac{\partial y}{\partial t} = -V_n \frac{1}{g} \frac{\partial x}{\partial r},$$

where the normal velocity is given by

$$V_n = \epsilon D \frac{1}{g}\frac{\partial}{\partial r}\left(\frac{1}{g}\frac{\partial K}{\partial r}\right) + J - \delta K \tag{2.25}$$

and the metric function and the curvature by

$$g = \sqrt{\left(\frac{\partial x}{\partial r}\right)^2 + \left(\frac{\partial y}{\partial r}\right)^2}, \quad K = \frac{1}{g^3}\left(\frac{\partial^2 y}{\partial r^2}\frac{\partial x}{\partial r} - \frac{\partial^2 x}{\partial r^2}\frac{\partial y}{\partial r}\right). \tag{2.26}$$

We now have that $x = 1$ corresponds to $R(t)$ and the contact point (x_*, y_*) corresponds to $r = 0$, see Figure 1. The boundary conditions are:

$$\frac{\partial y}{\partial r}(r = R(t), t) = 0, \quad \frac{\partial^3 y}{\partial r^3}(r = R(t), t) = 0, \tag{2.27}$$

$$\frac{\partial y/\partial r}{\partial x/\partial r}(r = 0, t) = \tan\theta, \quad \text{if} \quad -d \le x_* < 0 \ \text{ and } \ y_* = \bar{h}_m, \tag{2.28}$$

$$\frac{\partial y/\partial r}{\partial x/\partial r}(r = 0, t) = \tan(\theta - 90^\circ), \quad \text{if} \quad x_* = 0 \ \text{ and } \ 0 \le y_* < \bar{h}_m.$$

and

$$\frac{1}{g}\frac{\partial K}{\partial r}(r = 0, t) = \frac{f_m}{\epsilon\beta}. \tag{2.29}$$

The initial condition is

$$y(r,0) = 0,\ x(r,0) = r,\ 0 \le r \le 1. \tag{2.30}$$

And, the nondimensional coordinates of the contact point satisfy

$$x_* = 0, \quad \text{if} \quad 0 \le y_* < \bar{h}_m, \tag{2.31}$$

$$y_* = \bar{h}_m, \quad \text{if} \quad -d \le x_* < 0.$$

3 Numerical method

Evolution of the crystal surface is solved by a finite-difference method. N marker particles are placed along the surface and advanced according to equations (2.24). Centered, second order accurate and conservative finite difference approximations are used for the spatial derivatives in (2.24); one-sided finite differences are used where needed to compute derivatives at the boundaries $r = 0$ and $r = R(t)$. This yields a set of coupled ordinary differential equations for the motion of marker particles. The time derivatives are approximated by the forward Euler method.

The computational cycle consists of the following steps:

- Given the coordinates (x, y) of marker particles at time t, compute g, K (including g_0 and K_0), the derivatives of curvature and then V_n in the interior points. K_0 is computed by imposing the boundary condition (2.29);
- Using Euler scheme, compute coordinates (x, y) of the interior marker particles at time $t + \Delta t$, where Δt is the time step;
- Taking into account (2.31) and using 2nd order accurate one-sided finite differences, compute coordinates x_*, y_* of the contact point at time $t + \Delta t$ from (2.28);
- Remesh, i.e. redistribute the marker particles along the surface in order to preserve uniform spacing. With this purpose, the parametric cubic spline representation of the curve is constructed. These splines are then used to redistribute the marker particles at evenly spaced arc lengths (also, the code has an option to dynamically increase the number of markers along the surface once it becomes too elongated).

The remeshing justifies the proper choice of the parametrization - it ensures the parameter is the arc length, $r = s$. Therefore, r lies in the time-dependent interval $[0, S(t)]$, where $S(t)$ is the total arc length of the curve. The remeshing procedure is computationally expensive but it ensures the smoothness of the surface for the entire simulation period. With this procedure, almost no "stretch" of the parametrization occurs and the metric function becomes unity everywhere in $[0, S(t)]$, except the very narrow region near $s = 0$ where the boundary pollutes the data. However, this error decreases rapidly with the grid refinement (see Figure 2(b)). The surface rearranges quickly at the junction point to satisfy the equilibrium contact angle θ with the mask at the contact point.

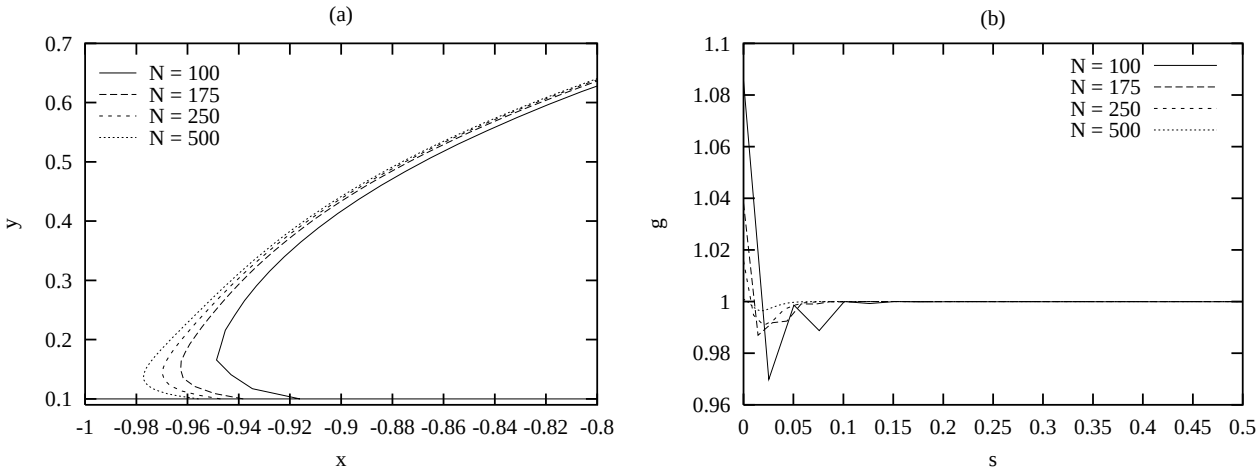

Figure 2: (a): Crystal surface at $t = 90$, computed with different number of marker particles (ref. Figure 3(b) for the values of parameters); (b): Corresponding metric functions $g(s)$.

To proove the validity of the numerical code, we made a series of runs with $N = 100, 175, 250, 500$ and, in Figure 2 plotted the surface profiles near the contact point and the corresponding metric functions (at $t = 90$, when the overgrowth on the mask is almost completed) for the case of Figure 3(b). The inspection of Figure 2 suggests that $N = 250$ marker particles provide accurate enough resolution of the curve; the difference in the x-coordinates of the contact point for $N = 250$ and $N = 500$ is 0.0085, and the deviation of $g(0)$ from unity for $N = 250$ is 1.6%. Thus, the computations presented in the Sections 4 and 5 were done with $N = 250$ marker particles. We verified all the results by performing runs with $N = 500$.

As a further check on the numerical code, we set $\delta = J = 0$ in (2.25), $f_m = 0$ in (2.29), $\bar{h}_m = 0$ in (2.28), (2.31) and computed (for different contact angles θ) the evolution of a retracting solid film step. We obtained the same surface profiles as in [29], where the latter problem is considered in detail (comparison not shown).

4 Numerical results for mask layer of nonzero thickness

As an example of the crystal surface evolution, Figure 3 shows the surface profiles for the contact angles $\theta = 30°$ and $\theta = 150°$ at different values of the nondimensional time (note the different scales along x and y-axis).

At later times, the curve in Figure 3(a) bends in the vicinity of the contact point, see Figure 4. This indicates that the crystal prefers not to "wet" the mask, i.e. the contact angles larger than 90° are preferred (as in Figure 3(b)). The contact angle is held constant along the mask surface during the computation except at the corner of the mask; for further detail see below.

Some comments should be made about the initial stage of the evolution from zero-level initial condition (2.30) and about the numerical treatment of the curve propagation over the

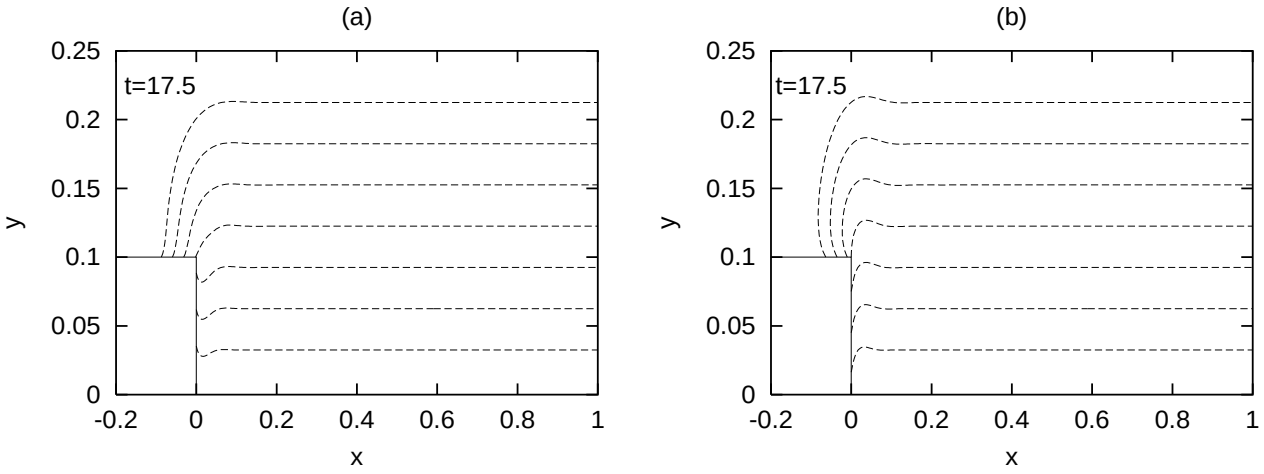

Figure 3: The evolving crystal surface. (a): $\theta = 30°$, (b): $\theta = 150°$. $L = \ell = 5$ μm, $h_m = 0.5$ μm. The surface profiles are dumped every 2500 time steps. The time labels correspond to the time at which the last profile is dumped. In (a) and (b), θ is the angle between the mask and the interior of the crystal at the contact point. The profiles shown at $t = 10$ (fourth from the bottom in (a) and (b)) have the contact point exactly on the mask corner where θ readjusts, ref. the discussion below.

step corner. First, note that initial condition (2.30) does not match the boundary condition (2.28). This implies that a singularity exists at $(x = 0, y = 0)$ at $t = 0$. This singularity does not present a barrier in solving the system numerically. Physically, the equilibrium angle should be formed instantaneously compared to the time needed for the evolution of the surface. We are not concerned with the details of this instance. Our numerical experiments reveal that for some values of nondimensional parameters the contact point initially retracts in the unphysical domain $y < 0$ (below the substrate, case $\bar{h}_m > 0$) or in the domain $x > 0$ (on the substrate, case $\bar{h}_m = 0$). If this happens we replace the initial curve (2.30) with the hyperbolic tangent curve having the desired contact angle θ with the mask at the contact point. For instance, in the case of Figure 3(a) this curve may be

$$y(r,0) = y_0 \left(1 - \tanh\left(r\frac{\tan\theta}{y_0}\right)\right),\ x(r,0) = r,\ 0 \le r \le 1 \tag{4.1}$$

where, y_0 gives the small initial elevation of the surface at $x = 0$. Similarly, in the case of Figure 3(b) the initial condition may be

$$y(r,0) = y_0 \tanh\left(r\frac{\tan\theta}{y_0}\right),\ x(r,0) = r,\ 0 \le r \le 1 \tag{4.2}$$

where, y_0 gives the small initial elevation of the surface at $x = 1$.

Similar reasoning is applied to the step corner point. Numerically, the corner point is singular in the sense that the contact angle is not well defined there. One way to deal with this situation is to instantly readjust the angle the curve forms with the upper mask surface to the equilibrium value once the contact point reaches the step corner. However, such

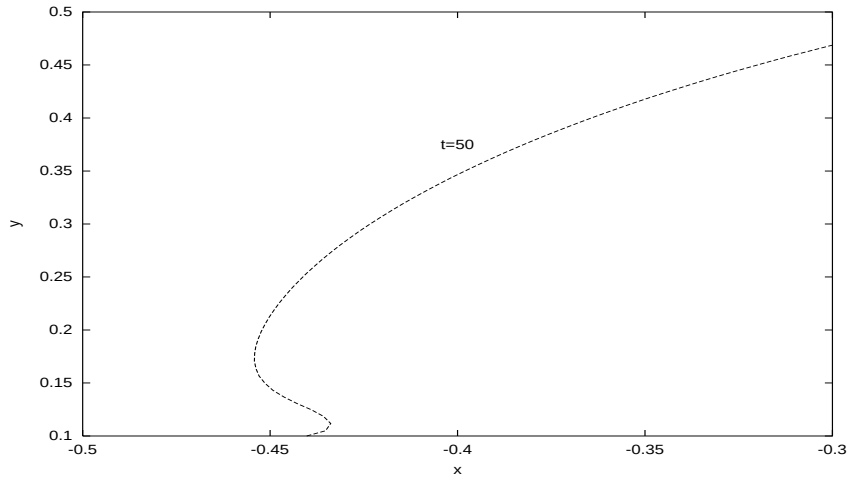

Figure 4: Snapshot of the crystal surface shown in Figure 3(a) at $t = 50$.

instant readjustment causes a short retraction into the unphysical domain ($x > 0, y = \bar{h}_m$). To avoid this retraction, we pin the contact point at the corner and allow the contact angle with respect to the upper mask surface to readjust to the equilibrium contact angle there. Once the desired angle is reached, the contact point resumes motion along the mask. The time interval needed for the readjustment is vanishingly small compared to the characteristic times of the problem. These times are as follows.

- T_1 = the time needed for the "bump" on the surface to disappear. T_1 is an important quantity since in semiconductor device manufacture one may not want to grow the crystal with deformed surface; also, T_1 is interesting since it provides some measure of surface diffusion's effect on the evolution.

- T_2 = the time needed for the contact point to reach the point ($x = -d, y = \bar{h}_m$) on the mask i.e., reach the end of the mask region.

- T_3 = the time needed for the contact point to reach the step corner (only in the case $h_m > 0$).

We also define:

- the normalized contact point position as the ratio of the distance (along the x-axis, from the contact point to the origin) to the mask region width, i.e. $|x_*|/d$;

- the normalized maximum growth thickness as the ratio of the maximal elevation of the surface (the "bump" height) to the height of the crystal at $x = 1$.

Figure 5(a) shows the normalized contact point position *vs.* contact angle at $t = T_1$. The crystal overgrowth onto the mask increases as the contact angle increases (compare to Figure 3(a),(b) where, at the same times, the overgrowth is approximately the same but the "bump" is more pronounced for $\theta = 150°$, therefore resulting in larger overgrowth at $t = T_1$). The value of T_1 depends on the relative tolerance chosen to measure the disappearence of

the "bump"; for instance, with the relative tolerance 0.005 used to compute the curve in Figure 5(a) and for $\theta = 150^\circ$ (case of Figure 3(b)) the value for T_1 is 73.3.

Figure 5(b) shows the normalized maximum growth thickness *vs.* mask thickness at $t = T_3$ for contact angles $\theta > 90^\circ$. The graphs for contact angles $\theta < 90^\circ$ are not shown since, as Figure 3(a) suggests, the maximum elevation of the surface can occur at the contact point as well as at the "bump" - thus sometimes making it difficult to distinguish between these two cases. The normalized maximum growth rate decreases with the mask thickness because the "bump" smooths out as the crystal grows vertically. The value of T_3 depends on the mask thickness; for the case of Figure 3(b), $T_3 = 9.5$.

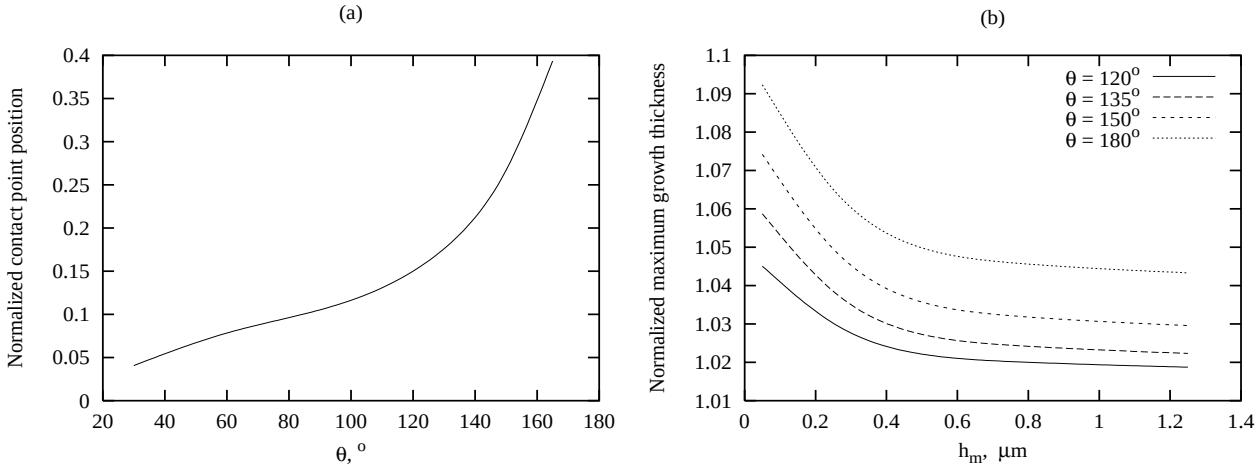

Figure 5: (a): Normalized contact point position *vs.* contact angle at $t = T_1$. $L = \ell = 5$ μm, $h_m = 0.5$ μm. (b): Normalized maximum growth thickness *vs.* mask thickness at $t = T_3$ for different contact angles; L, ℓ are the same as in (a).

The numerical experiments described in this section and in Section 5 were run on a single 300 MHz R12000 CPU on an SGI Origin 2000 Workstation. The computational times depend strongly on h_m, L and ℓ but they never exceeded 1 hour.

5 Numerical results for mask layer of zero thickness

In this section, we set $\bar{h}_m$ to zero in the boundary conditions (2.28), (2.31) and again solve the resulting initial/boundary value problem for the evolution equations (2.24) numerically.

Figure 6(a) shows the example of the crystal surface at time T_1 for different contact angles. The corresponding curvatures as functions of the arc length are shown in Figure 6(b). The spikes on the graphs of $K(s)$ correspond to the regions in the vicinity of the contact point on the graphs of the surface where curves are bent to satisfy the equilibrium contact angle boundary condition. The inflection points located at $x \approx 0.08,\ 0.11,\ 0.12$ (immediately after the smoothed "bump") on the graphs of the surface for $\theta = 30^\circ,\ 90^\circ,\ 150^\circ$ respectively correspond to $s \approx 0.39,\ 0.84,\ 1.33$ (the last point not shown) on the graphs of $K(s)$.

In Figures 7, 8 we study the dependence of the ELOG characteristics on widths of the mask and the substrate regions, ℓ and L.

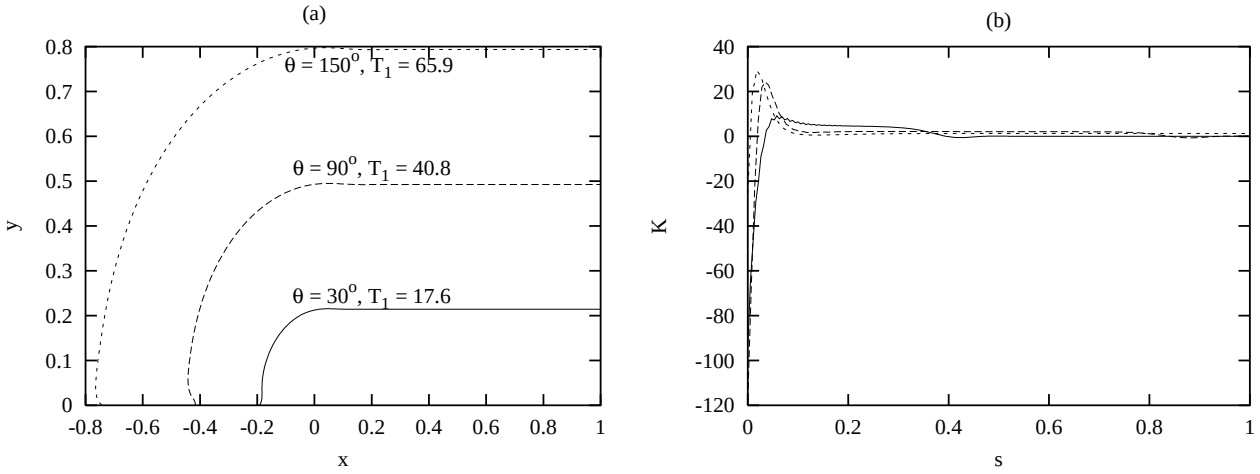

Figure 6: (a): Graphs of the crystal surface at times the "bump" is considered to have disappeared, for different contact angles. $L = \ell = 5$ μm, $h_m = 0$. (b): Curvatures of the curves in (a) as functions of the arc length.

Figure 7 shows the dependence of the normalized position of the contact point on ℓ and L. As in the case of the mask layer of nonvanishing thickness, the overgrowth onto the mask is larger for larger contact angles. For a given contact angle, the overgrowth decreases with increasing ℓ and L, with the dependence of the overgrowth in Figure 7(b) on L being approximately linear. Note that the variation in ℓ has stronger impact on the overgrowth than the variation in L. Figure 7(a) suggests that wider mask regions will result in the saturation of the overgrowth. This conclusion is consistent with the model. Indeed, the surface diffusion flux from the mask onto the growing crystal is the driving force for ELOG, with another component of the driving force being the constant flux of atoms from the vapor on the crystal surface. The flux on the mask is given by (2.23) and it saturates as $d = \ell/L$ increases (the close-to-linear dependence of the ELOG on L can't be easily explained since all nondimensional parameters of the problem are functions of L, ref. Table 3).

Figure 8 shows the similar dependence of the normalized maximum growth thickness on ℓ and L and the same explanation applies to the curves in Figure 8(a). It is interesting that the characteristic time T_2 does not depend on the contact angle. That is, having L fixed, the time needed for ELOG over the distance ℓ is independent on the ratio of the crystal to the mask surface energies (for the case of Figure 6(a), $T_2 = 87$).

Film thickness at the center of the substrate region ($x = L$) as a function of ℓ and L is shown in Figure 9. Film thickness increases with ℓ, and the rate of the increase decreases as the contact angle increases (Figure 9(a)). Film thickness linearly decreases with L (also with decreasing rate with respect to the increase of the contact angle, Figure 9(b)).

Film thickness at the center of the substrate region increases essentially linear in t', with rate ≈ 1 μm/min. There is no dependence of the growth at substrate center on the contact angle.

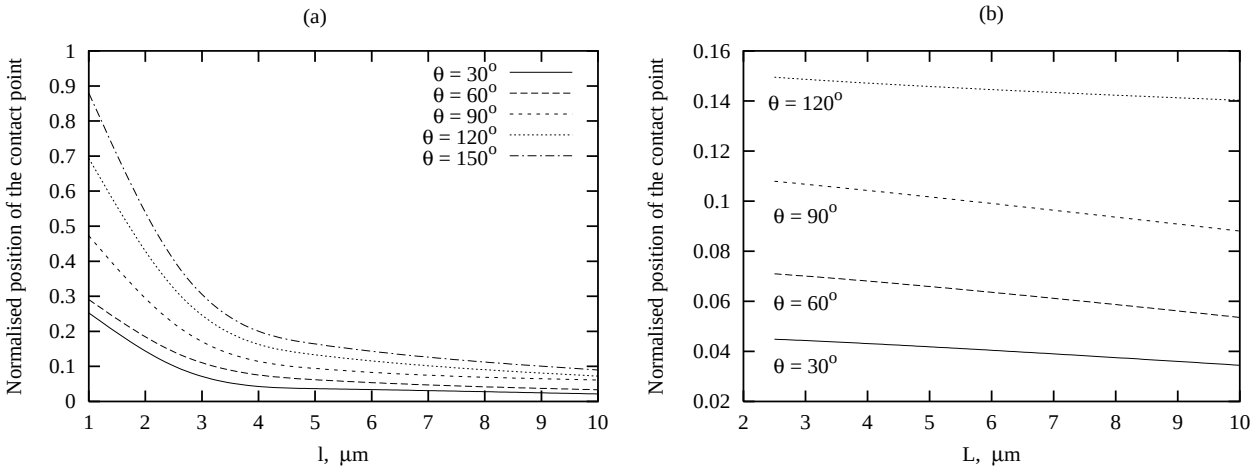

Figure 7: (a): Normalized position at $t = T_1$ of the contact point *vs.* mask region width, for different contact angles. $L = 5$ μm, $h_m = 0$. (b): Normalized position (at $t = T_1$) of the contact point *vs.* substrate region width, for different contact angles. $\ell = 5$ μm, $h_m = 0$. For the representative values of T_1 refer to Figure 6(a).

6 Discussion and conclusions

We developed a model for the epitaxial semiconductor crystal growth on a masked substrate in a surface diffusion-limited growth regime.

In this model, the overgrowth of the crystal on the mask (as well as growth in vertical direction) is a dynamic process which depends on many factors, such as the height of the mask above the substrate, the widths of masked and open regions, the ratio of mask to substrate surface tensions, etc. Unlike Type 1 and Type 2 models cited in the Introduction, our model does not assume the overgrowth or lack of the overgrowth *a priori*, while in these models the assumption is made based on results of specific experiment which the model aims to describe. Despite the fact that numerical results presented in Sections 4 and 5 always exhibit the overgrowth, the trial runs with anisotropy included in the model indicated that the overgrowth could be suppressed by selecting the degree of anisotropy and the fast growth directions [21].

The predictions of the modeling compare favorably to the results obtained by other authors. The region of enhanced growth near the contact point ("bump") shown in Figure 3 supports the experimental and theoretical evidence for the surface diffusion on the mask to contribute strongly to such enhanced growth [5, 7, 11], [17]-[19]. Eventually, the "bump" is smoothed out by the surface diffusion on the crystal surface.

The profiles of the crystal surface we obtained show close resemblance to experimental profile in Figure 5(b) of [3] and to experimental profiles in Figures 4 and 5 of [7]. To make such comparison, our computed profiles should be truncated, at some given time, with imaginary vertical line passing to the left of the "bump" maxima. The right part of the profile is then shifted to the right so that the left endpoint stays on the vertical line at $x = 0$ (to account for the lack of the overgrowth in the works cited). The detailed comparison with these and other experimental works is, however, impossible since the natural anisotropy of the crystal

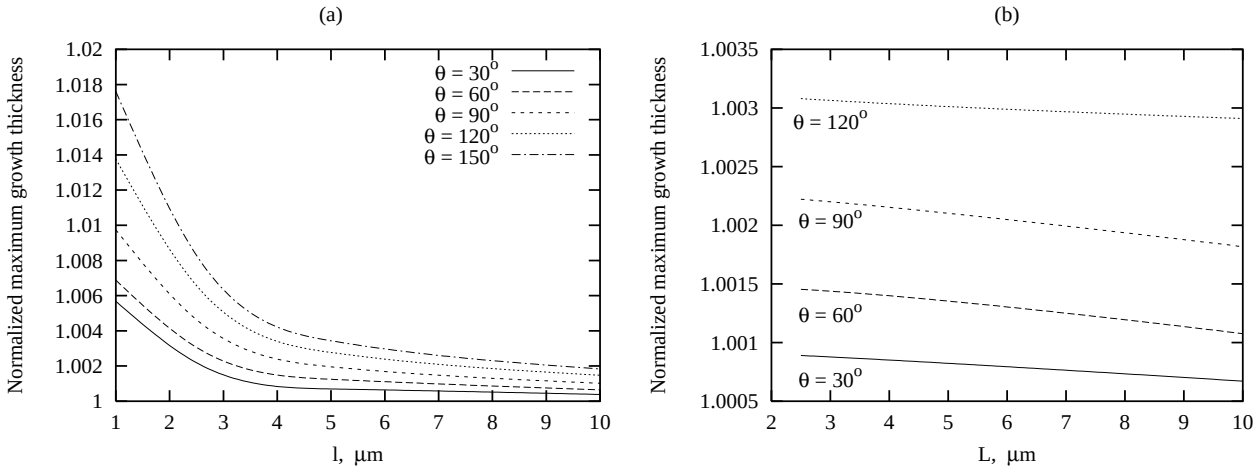

Figure 8: (a): Normalized maximum growth thickness (at $t = T_2$) *vs.* mask region width, for different contact angles. $L = 5\ \mu$m, $h_m = 0$. (b): Normalized maximum growth thickness (at $t = T_2$) *vs.* substrate region width, for different contact angles. $\ell = 5\ \mu$m, $h_m = 0$.

growth is not accounted for in this study.

The linear dependence of the normalized maximum growth thickness and of the film thickness at the center of the substrate region on the width of the substrate region L (ref. Figures 8(b), 9(b)) was found experimentally in [7] for the surface diffusion dominated growth. Also, Figure 9(a) shows that the film thickness at the center of the substrate region monotonically increases with the mask width ℓ due to the increase of the lateral source supply . This result is well known [3, 11, 17]. Again, similar dependence was found experimentally in [11] for the surface diffusion dominated growth. Note that the normalized maximum growth thickness in Figure 8(a) decreases with ℓ despite that the film thickness at $x = L$ increases with ℓ. The reason is that surface diffusion along the crystal surface has a strong smoothing effect in the regions of the surface where the curvature is large.

Future directions for the research include considering anisotropic growth, the diffusion in the vapor and the application of external fields. The first of these results is already in hand, and will be reported elsewhere [21].

Acknowledgements

M. Khenner and R.J. Braun were supported by NSF Grants DMS-9631287 and DMS-9722854. This problem is an outgrowth of one studied in the 15th Annual Mathematical Problems in Industry Workshop held in 1999. The authors thank G. Berensel, K. Brattkus, L.P. Cook, A.D. Fitt, D.A. French, S. Kim, J.R. King, A.A. Lacey, J. Pelesko, D. Petrasek, C. Please and A. Roosen for helpful conversations. M.G. Mauk wishes to acknowledge support of the Ballistic Missile Defense Organization under Small Business Innovation Research contract DASG60-92-C-004.

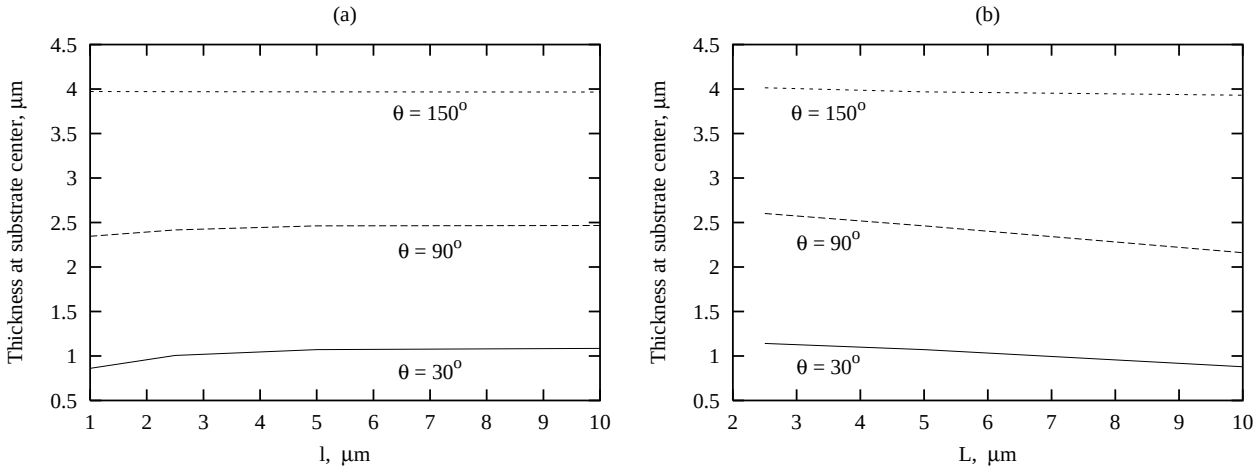

Figure 9: (a): Thickness at substrate center (at $t = T_1$, ref. Figure 6(a)) *vs.* mask region width, for different contact angles. $L = 5$ μm, $h_m = 0$. (b): Thickness at substrate center at $t = T_1$ *vs.* substrate region width, for different contact angles. $\ell = 5$ μm, $h_m = 0$.

References

[1] M. Aoki, H. Sano, M. Suzuki, M. Takahashi, K. Uomi and A. Takai, *Electron. Letters* 27 (1991) 2138.

[2] H. Okumura, N. Saito, J.-I. Kusano, T. Aida, F. Sato, K. Takizawa *Jpn. J. Appl. Phys.* 37 (1998) L484.

[3] E.J. Thrush, J.P. Stagg, M.A. Gibbon, R.E. Mallard, B. Hamilton, J.M. Jowett and E.M. Allen, *Materials Science and Engineering* B21 (1993) 130.

[4] D.A. French, J. Pelesko and R.J. Braun, *Final Reports of the 15th Annual Workshop on Mathematical Problems in Industry*, University of Delaware (1999).

[5] M.A. Gibbon, J.P. Stagg, C.G. Cureton, E.J. Thrush, C.J. Jones, R.E. Mallard, R.E. Pritchard, N. Collis and A. Chew, *Semicond. Sci. Technol.* 8 (1993) 998.

[6] C.C. Mitchell, M.E. Coltrin, J. Han, *Journal of Crystal Growth* 222 (2001) 144.

[7] T. Sasaki, M. Kitamura, I. Mito *Journal of Crystal Growth* 132 (1993) 435.

[8] B. Korgel, R.F. Hicks, *Journal of Crystal Growth* 151 (1995) 204.

[9] D.G. Coronell, K.F. Jensen, *Journal of Crystal Growth* 114 (1991) 581.

[10] O. Kayser, *Journal of Crystal Growth* 107 (1991) 989.

[11] Y. Sakata, Y. Inomoto, K. Komatsu, *Journal of Crystal Growth* 208 (2000) 130.

[12] O.-K. Nam, T.S. Zheleva, M.D. Bremser, R.F. Davis, *Journal of Electronic Materials* 27(4) (1998) 233.

[13] P. Fini, H. Marchand, J.P. Robertson, S.P. DenBaars, U.K. Mishra, J.S. Speck, *Journal of Crystal Growth* 209 (2000) 581.

[14] D. Marx, Z. Kawazu, T. Nakayama, Y. Mihashi, T. Takami, M. Nunoshita, T. Ozeki, *Journal of Crystal Growth* 289/190 (1998) 87.

[15] K. Hiruma, T. Haga, M. Miyazaki, *Journal of Crystal Growth* 102 (1990) 717.

[16] S. Sudo, Y. Yokoyama, T. Nakazaki, K. Mori, K. Kudo, M. Yamaguchi, T. Sasaki, *Journal of Crystal Growth* 221 (2000) 189.

[17] J.E. Greenspan, X. Zhang, N. Puetz, B. Emmerstorfer, *J. Vac. Sci. Technol. A* 18(2) (2000) 648.

[18] T. Fujii, M. Ekawa, S. Yamazaki, *Journal of Crystal Growth* 146 (1995) 475.

[19] M.F. Zybura, S.H. Jones, *J. Electron. Mater.* 23(10) (1994) 1055.

[20] L.J.M. Bollen, C.H.J. Van Den Brekel, H.K. Kuiken, *Journal of Crystal Growth* 51 (1981) 581.

[21] M. Khenner, R.J. Braun, M.G. Mauk, in preparation.

[22] S. Osher, J.A. Sethian, *J. Comput. Phys.* 79 (1988) 12.

[23] T. Nishinaga, *Handbook of Crystal Growth* 3 (1994) 666 (ed. D.T.J. Hurle, Elsevier Science).

[24] A.A. Chernov, *Handbook of Crystal Growth* 3 (1994) 458 (ed. D.T.J. Hurle, Elsevier Science).

[25] T. Nishinaga, X.Q. Shen, *Advances in the Understanding of Crystal Growth Mechanisms* (1997) 117 (ed. T. Nishinaga et al., Elsevier Science).

[26] C. Herring, *Structure and Properties of Solid Surfaces* 5 (1952) (ed. R. Gomer and C.S. Smith, The University of Chicago Press).

[27] W.W. Mullins, *J. Appl. Phys.* 28(3) (1957) 333.

[28] J.A. Sethian, *Comm. Math. Phys.* 101 (1985) 4.

[29] H. Wong, P.W. Voorhees, M.J. Miksis, S.H. Davis, *Acta Mater.* 48 (2000) 1719.